Effects of Callus and Bonding on Strains in Bone Surrounding an Implant Under Bending

Sarandeep S. Huja, BDS, MDS, MS*/Haihong Qian, MSME**/
W. Eugene Roberts, DDS, PhD***/Thomas R. Katona, PhD, DMD****

Descriptions of the healing and adaptation of endosseous implants have been provided; however, their effects on mechanical parameters such as maximum and minimum principal strains, strain energy density, and maximum shear strain have not been addressed. Three linear, elastic, and partially anisotropic finite element models were generated to simulate the immediate postoperative period, time of provisional loading, and long-term adaptation of bone surrounding implants. In each model, unbonded and bonded interface conditions were imposed. Bone geometry was estimated from dental implants placed in femurs of hounds. A lateral load was applied and the mechanical parameters were calculated. Interface bonding decreased the peak minimum principal strain 2.6 to 6.4 fold, while the presence of a callus reduced it 3 to 7 fold. These data document the critical stabilizing roles of callus and bond formation.
(Int J Oral Maxillofac Implants 1998;13:630–638)

Key words: adaptation, endosseous implant, finite element model, strain

Endosseous implants have been used successfully for a variety of applications in dentistry[1,2] and orthopedics.[3] However, the scientific basis for the rigid ("osseointegrated") interface has developed slowly[4] because of an incomplete understanding of relevant bone physiology.[5,6]

The processes involved in bone adaptation to an endosseous implant have been described.[7] The healing response includes the formation of calluses and a mechanism for generating a vital interface between implant and bone. Rapid remodeling of bone near the interface has been shown consistently.[5] It was expected that this rapid turnover would lead to a change in bone mechanical properties. Recently, microhardness of different bone types in various regions surrounding an implant have been evaluated.[8] These data suggest that bone near the implant has distinctly different mechanical properties than cortical bone away from the implant. Also, it has been reported that endosseous implants bond to bone. The exact nature of this bond is unknown, but it is likely a combination of mechanical interlocking and intermolecular forces. These adaptational responses and bonding conditions at the implant-bone interface are certain to affect mechanical parameters[9–11] (eg, maximum and minimum principal strains and strain energy density) that are typically used to analyze loaded biologic structures. However, limited information is available on how these mechanical parameters change during healing and long-term adaptation. The purpose of this study was to use finite element (FE) methods to isolate the effects of callus formation and bonding on the mechanical environment in implant-supporting bone.

*Graduate Student, Section of Orthodontics, Oral Facial Development, Indiana University School of Dentistry, Indianapolis, Indiana.
**Graduate Student, Department of Mechanical Engineering, Purdue University, School of Engineering and Technology, Indiana University-Purdue University at Indianapolis, Indiana.
***Professor, Section of Orthodontics, Physiology and Biophysics and Mechanical Engineering, Indiana University Schools of Dentistry and Medicine, Indianapolis, Indiana; Purdue University, School of Engineering and Technology, Indiana University-Purdue University at Indianapolis, Indiana; University of Lille School of Medicine, Lille, France.
****Associate Professor, Section of Orthodontics and Mechanical Engineering, Indiana University School of Dentistry, Indianapolis, Indiana; Purdue University, School of Engineering and Technology, Indiana University-Purdue University at Indianapolis, Indiana.

Reprint requests: *Dr T. R. Katona, Biomechanics Research Laboratory, Room 250/A, Indiana University School of Dentistry, 1121 West Michigan Street, Indianapolis, Indiana 46202. E-mail: tkatona@iusd.iupui.edu*

Materials and Methods

Three convergent sets of FE models were developed, each simulating a stage of healing and adaptation (Figs 1 and 2). The model geometry was developed for a study in progress in which dental implants were placed for a 12-week period in the midfemoral diaphysis of mature hounds. Figure 1 is a cut-away schematic showing model dimensions.

The first model, nonadapted (NA), is an immediate post-placement simulation (Fig 2a). The implant in this model is surrounded by cortical bone that has not had the opportunity to adapt. The second model, adapted (AD), represents bone that was allowed to heal for 12 weeks (Fig 2b), ie, one canine remodeling cycle.[13] This is the waiting period after which provisional loading commences in clinical situations. The implant was surrounded by new bone adjacent to the implant and by calluses on the periosteal and endocortical surfaces. The three layers of new bone were meshed to represent the rapid remodeling gradient that is seen within about 1 mm of the interface. Each layer was given different material properties. The endosteal callus was meshed to fill the space between the endocortical bone surfaces and the implant. The third model, long-term adaptation (LA), is a hypothetical case simulating resorption of callus that accompanies long-term adaptation (Fig 2c). This model is identical to AD except that it lacks calluses. Change in cortical bone dimensions related to expected bone modeling during long-term adaptation was not simulated.

Bonded versions of NA and LA consisted of 5,344 elements and 6,340 nodes. The corresponding unbonded models had 6,106 elements and 7,012 nodes. Bonded AD had 7,104 elements and 7,938 nodes. Unbonded AD had 8,640 elements and 9,474 nodes. All models were generated through PATRAN (PDA Engineering, Costa Mesa, CA) and solved through ABAQUS (Hibbit, Karlson and Sorensen, Providence, RI). All elements were eight-noded bricks. In each model, two interface conditions were imposed. A model was either entirely unbonded or fully bonded. Absence of bond between implant and bone was simulated with contact pairs.[14] These elements transmit compressive stresses but allow for separation under tension and sliding under shear. All unbonded models were idealized as frictionless. A cantilever bending load of 100 N at 13 mm from the periosteal surface of cortical bone was applied to each of the three models. This approximates the distance from the occlusal contact of a maxillary incisor to the crest of the alveolar bone.[15] Fixed displacement boundary conditions were applied to the undersurface of the cut cortical bone. In all instances, the same boundary and load conditions were imposed.

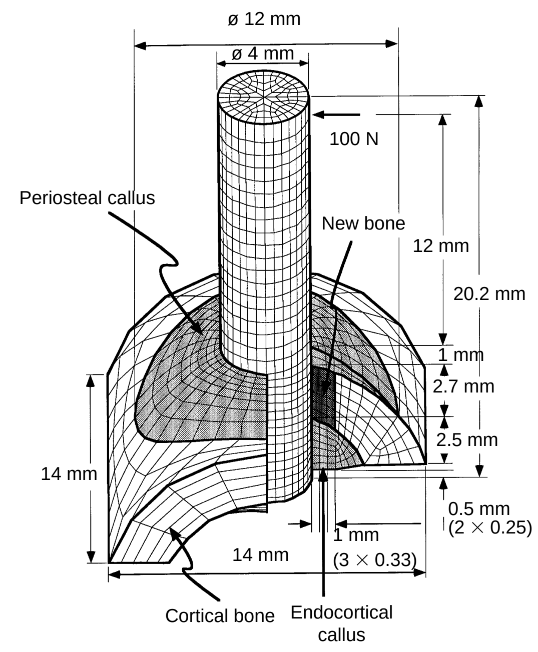

Fig 1 Geometry, finite element model, and mesh of adapted (AD) model. 100 N load is applied 13 mm from the periosteal side of the cortical bone. The AD model contains different types of bone: periosteal callus, endosteal callus, three layers of new bone in cortex surrounding implant and orthotropic cortical bone. The long-term adaptation (LA) model is the same, except it does not contain either type of callus. The nonadapted (NA) model is identical to the LA model but the implant is surrounded by orthotropic cortical bone only. The time sequence of adaptation is represented by NA to AD to LA.

Material properties (Table 1) of orthotropic canine cortical bone were estimated from the literature.[16] Elastic moduli in the three orthogonal directions were based on ratios of E_{rad}:E_{tan}:E_{long} = 0.65:0.8:1.[16] No estimates for the elastic moduli of the calluses and implant-adjacent adapted bone are available. Thus, material property distribution was approximated from the microhardness gradient previously demonstrated.[8] Poisson's ratio of 0.34 was chosen for all bones. All bone types were considered to be linear, elastic, and homogenous. Material properties for titanium were E = 104 GPa and $\upsilon = 0.36$.[17]

It is important to emphasize that the geometry and mechanical properties used in these models simulate implants in dog femoral cortex. Because of the vast differences in the thickness, geometry, porosity, vascularity, and mechanical properties of the bone, no direct comparisons of results can be made to implants placed in the maxilla or mandible. Such differences exist between the anterior and posterior parts of each jaw, thus making within-jaw comparisons difficult to generalize. Thus, in this study, only *relative* comparisons are made between models.

The peak values of four mechanical parameters—minimum principal strain (MIN), maximum principal strain (MAX), strain energy density (SED), and maximum shear strain (MSS)—were obtained from the FE models. In this study, MIN was always compression and MAX was always tension. The nodes along the length of the implant were divided into seven groups that extended from the periosteal surface to the endocortical surface of the bone for NA and LA. Because the calluses were present, there were 16 such groups for AD. Each group consisted of 17 nodes about the circumference of the implant's interface. As an example, the desired values of strain energy density (SED) in bone were obtained as follows. In each group along the length of the implant, the peak value (SED_p) of strain energy density from the 17 circumferential nodes was identified. For comparisons, the highest value of strain energy density (SED_{pmax}) among the 7 (NA and LA) or 16 (AD)

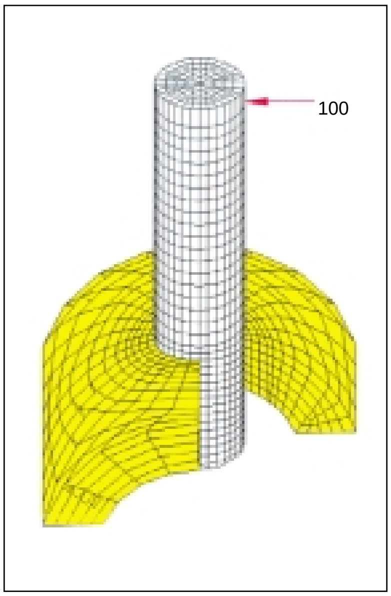

Fig 2a Finite element model of the nonadapted (NA) model. The unbonded version simulates an immediate postoperative implant. Only cortical bone *(yellow)* surrounds the implant. The bonded version of NA is hypothetical.

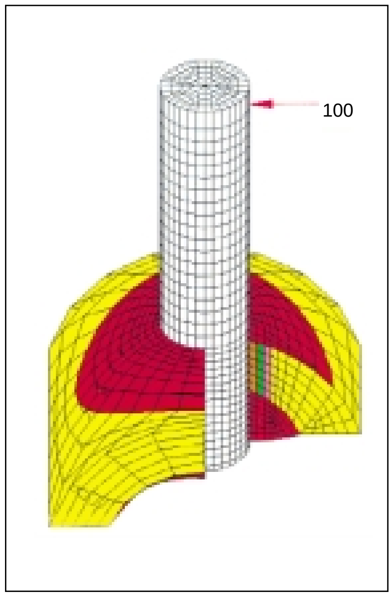

Fig 2b Finite element model of the adapted (AD) model. The two versions, unbonded and bonded, simulate adapted bone 12 weeks postimplantation. Three layers (a, b, c) of increasingly stiff new bone surrounding the implant are shown in different colors. Periosteal and endosteal calluses *(red)* are included.

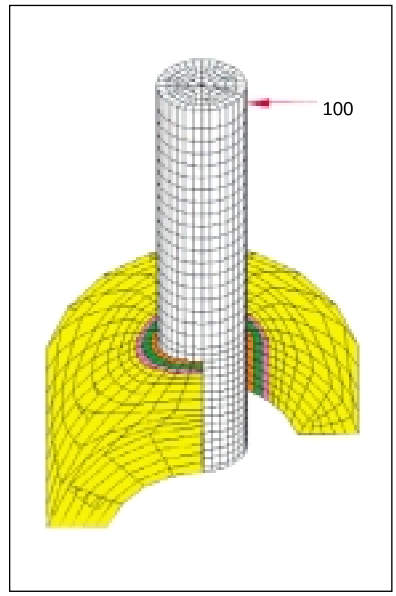

Fig 2c Finite element model of the long-term adaptation (LA) model. Three layers of new bone surround the implant. Cortical bone *(yellow)* is 1 mm from the implant interface. This model lacks the calluses of the AD model.

Table 1 Material Property Parameters for Bone and Implant

Bone type and material	Young's modulus (GPa)			Shear modulus (GPa)		
Periosteal callus	4			—		
Endosteal callus	4			—		
New bone—layer c	8			—		
New bone—layer b	7			—		
New bone—layer a	4			—		
Titanium	104			—		
Cortical bone	E_{long}	E_{tan}	E_{rad}	G_{rt}	G_{rz}	G_{tz}
	13.5	10.8	8.8	3.1	3.8	4.5

Longitudinal (long) refers to the long axis of the femur; radial (rad) indicates the outward direction from the center of the femur; the tangential (tan) direction is tangent to the outer surface of the femur.

peak values thus obtained was used. For further comparisons, the highest peak values of the mechanical parameters in each of these models was normalized with the corresponding highest peak value of unbonded NA (eg, SED_{pmax} in AD/SED_{pmax} in NA). NA was chosen because it corresponds to the time that implants are placed at initial surgery and forms the baseline from which comparisons can be made. In addition to comparisons of peak parameter values, their locations were also investigated.

Results

Healing, as defined herein, consists of two processes: *(1)* formation of calluses and new bone around the implant (modeling and remodeling events), and *(2)* formation of a bond between implant and bone. In laboratory experiments, the latter is indicated by an increase in interfacial bond strength. The effects of healing are depicted by comparing the unbonded nonadapted model (NA) with the adapted model (AD) in Figs 3 and 5. Calluses, new bone around the implant, and full bond between implant and bone decrease MIN_{pmax} by nearly one order of magnitude (8.3 fold). When unbonding at the interface of AD model was simulated, MIN_{pmax} decreased by only 3 times when compared to unbonded NA. Similarly, when unbonded NA is compared with unbonded or bonded AD, a dramatic decrease in MAX_p, SED_p, and MSS_p is also apparent (Figs 3b through 3d and 5).

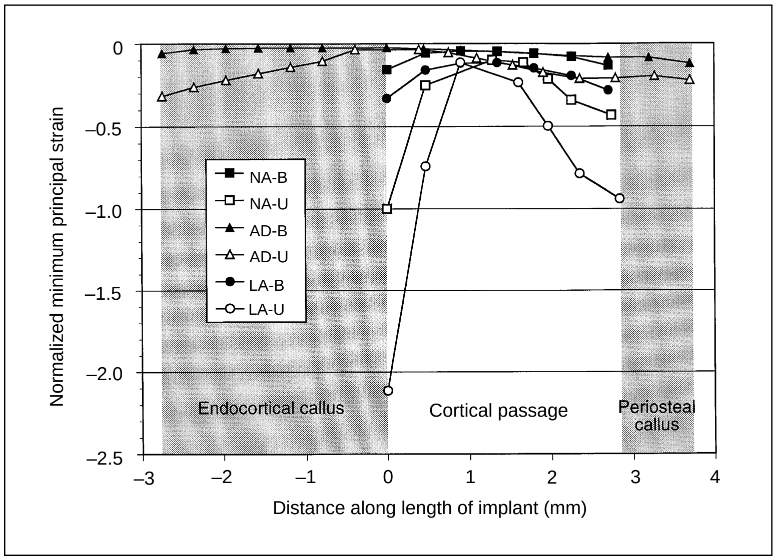

Fig 3a Peak values of minimum principal strain (MIN_p) at various node groups along the length of the implant normalized to the highest peak (MIN_{pmax}) for unbonded NA. B *(solid symbols)* and U *(open symbols)* indicate bonded and unbonded, respectively, in Figs 3a to 3d.

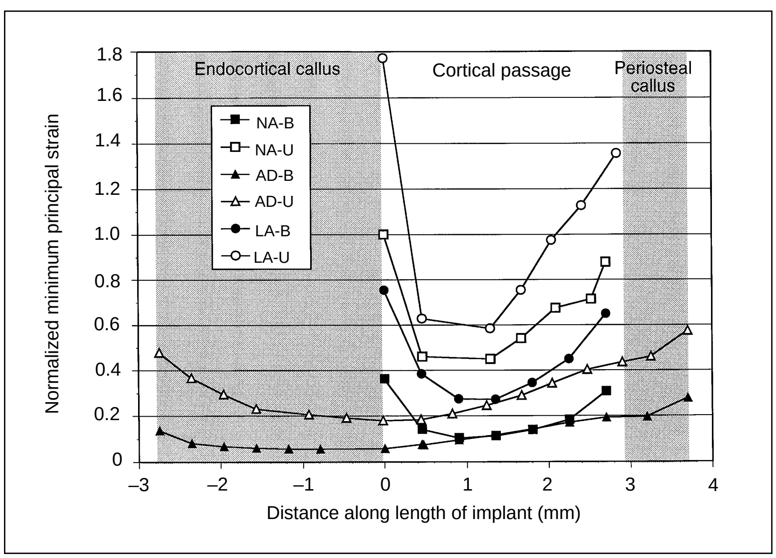

Fig 3b As in Fig 3a, but for the maximum principal strain (MAX_p).

The importance of the calluses was assessed by comparing AD with LA. Callus resorption and lack of a bond increased MIN_{pmax} by 6.6 fold (Figs 3a and 5). In contrast, MIN_{pmax} in the bonded cases increased 2.7 fold. This is also illustrated when various other mechanical parameters are compared (Figs 3 and 5). Values of parameters for LA (both bonded and unbonded) are higher than their corresponding values in AD.

Development of an interface bond decreased MIN_{pmax} 6.2 fold in NA and 6.4 fold in LA. However, bonding the implant to bone in AD decreased MIN_{pmax} only 2.6 times. For all four mechanical parameters, bonded AD had the lowest absolute values (Figs 3 and 5). Bonding decreases the values of all mechanical parameters investigated as compared to the values for their respective unbonded models.

The effects of healing, bonding (interface conditions), and callus resorption on peak maximum shear strain (MSS_p) in bone followed the same trend as MIN_p. However, the peak values of strain energy density (SED_p) were greatly affected by some of these variables of healing. For example, when comparing unbonded NA with unbonded AD, there was a 20-fold decrease in SED_{pmax} (Figs 3c and 5). Peak values of maximum principal strain (MAX_p) were less affected by healing for some of these comparisons. For example, MAX_{pmax} in AD was 3.1 fold less than in unbonded NA.

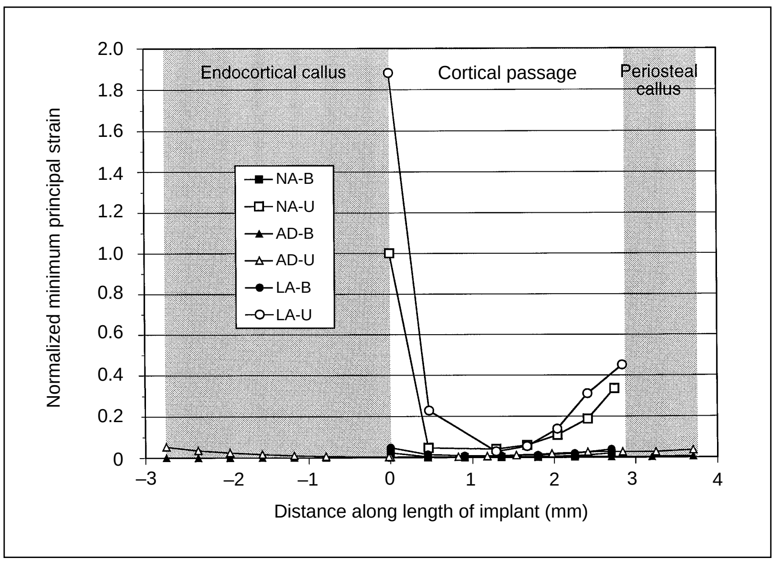

Fig 3c As in Fig 3a, but for strain energy density (SED_p).

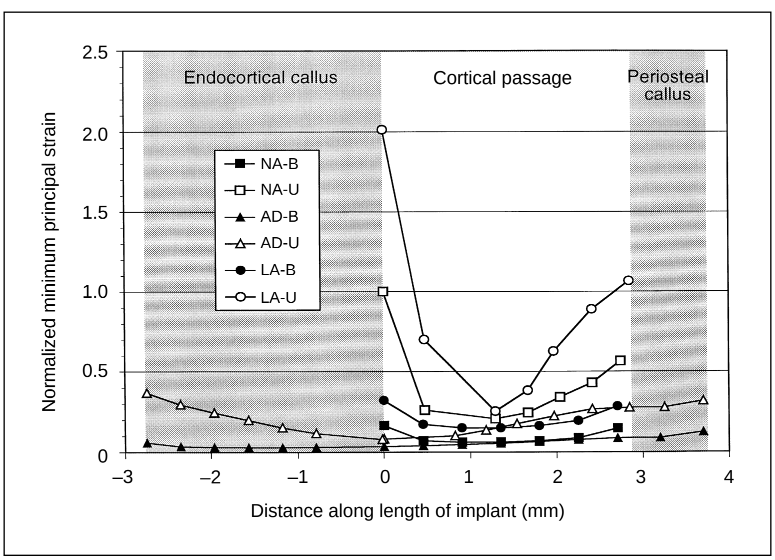

Fig 3d As in Fig 3a, but for maximum shear strain (MSS_p).

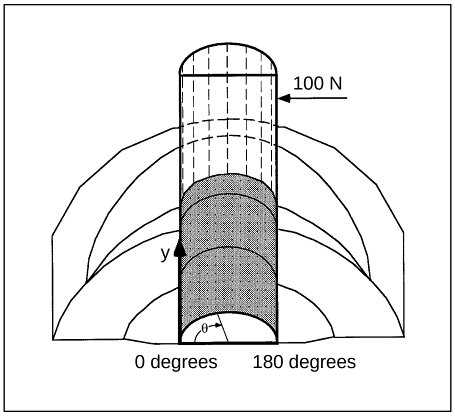

Fig 4a Cut-away schematic of adapted model (AD) depicting the coordinate system used in Figs 4b and 4c to locate peak values of mechanical parameters.

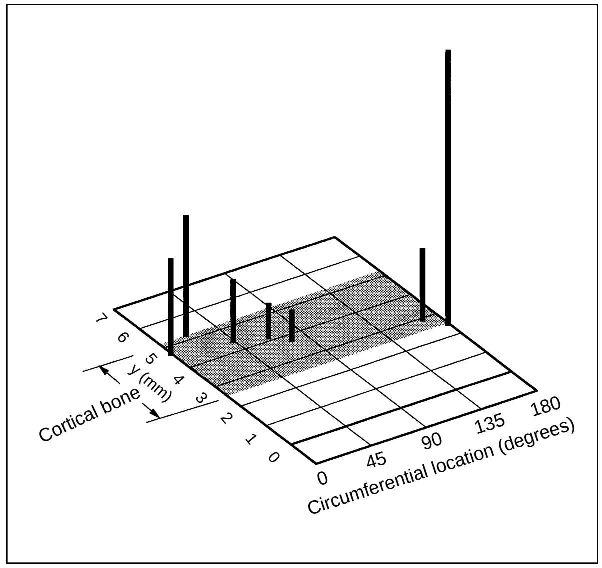

Fig 4b MIN_p at various groups of nodes for unbonded NA. MIN_{pmax} is located at the endocortical surface. Note the location of MIN_p at various node groups away from the bone surface.

Figures 4a to 4c depict the location of MIN_p for unbonded NA and bonded AD along the circumference of the implant for the various node groups. These simulated the two extreme conditions of adaptation. In unbonded NA, the highest value of MIN_p was located at the endocortical surface close to the plane of loading (Fig 4b). However, some of the other MIN_p values in groups of nodes were located at Θ other than 0 degrees and 180 degrees. In bonded AD, MIN_p was located essentially at Θ equal to 0 degrees or 180 degrees, while the highest value was located in the periosteal callus away from the plane of loading (Fig 4c). However, the value of MIN at Θ = 0 degrees was not very different (thin bar in Fig 4c). Similar trends were seen for MAX_p, SED_p, and MSS_p.

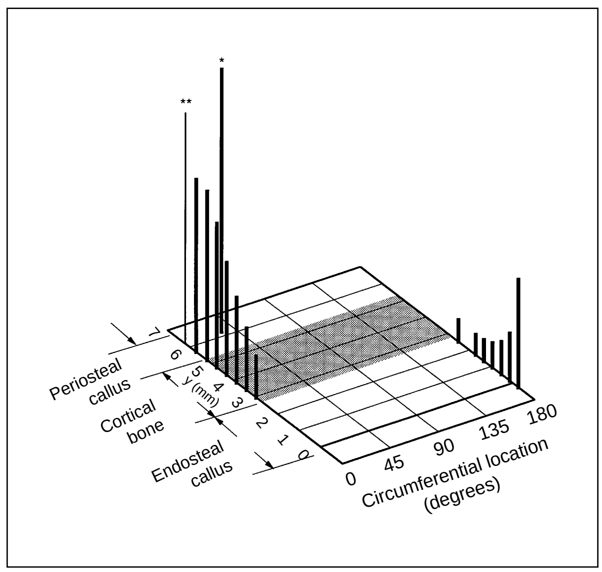

Fig 4c As in Fig 4b, but for bonded AD. Single asterisk indicates the highest peak value (0.0077) of MIN, which happens to be in the periosteal callus. Double asterisk is the value (0.0069) of MIN at Θ = 0 degrees *(thin bar)*, which is not very different from 0.0077.

Discussion

Finite element models in this study were used to provide relative estimates of the mechanical parameters under consideration. These estimates depend on the assumed material property values. Overestimation by studies using ultrasonic techniques[18] was taken into account in the selection of the elastic and shear moduli of canine cortical bone.[16] It is well known that bone is anisotropic and viscoelastic. Thus a limitation of this study is that bone was modeled as having isotropic and linear elastic properties, except for cortical bone, which was considered orthotropic. Others have also considered woven bone to be isotropic.[19] However, it is expected that with maturation of the callus by lamellar compaction and mineralization, it will develop anisotropy.[19] The only available estimate for the elastic modulus of fracture callus is through

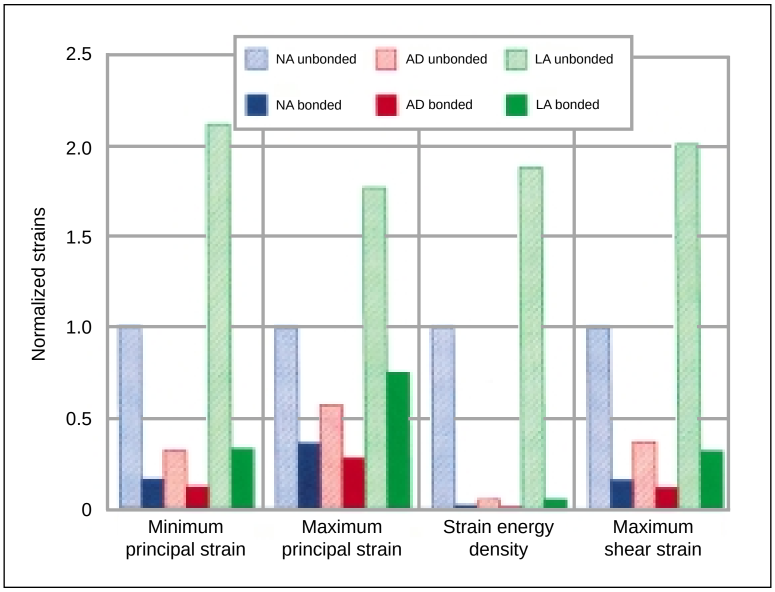

Fig 5 Normalized highest peak values (MIN_{pmax}, MAX_{pmax}, SED_{pmax}, MSS_{pmax}) of the four mechanical parameters relative to the respective pmax values of unbonded NA.

correlations with acoustic impedance.[20,21] However, it is possible that the healing and final resorption processes of calluses around endosseous implants are different from those in fracture callus, thus negating extrapolations. A distinct gradient of increasing microhardness has been shown to exist within 600 µm of the implant interface.[8] Also, a relationship between microhardness and elastic modulus has been demonstrated.[22,23] Bone adjacent to the endosseous implants remodels rapidly, and its osteonal nature is distinct.[7] Insufficient information was available to model the calluses and adjacent implant bone as anisotropic, although there are some observations of preferential orientation of osteons in this bone.[6,7] Therefore, based on previous histologic findings[7] and microhardness values,[8] estimates for the Young's modulus of bone within 1 mm of the implant interface and calluses were made (Table 1).

Canine long bones are frequent sites for the experimental placement of endosseous implants.[6,24] While in this study a load was applied at a specific location to simulate intraoral conditions, canine cortical bone material properties were used. This study has developed from another canine FE model that is currently being examined. While information on the orthotropic properties of the mandible is available, such data on the alveolar cortex are not. It is emphasized that in the present study only *relative* comparisons between models were made.

Considerable controversy exists in the literature on the ability of bone to bond to implant materials. Biocompatibility of the implant material, surface roughness, topology at the interface, and test methods are frequently cited as sources of this controversy.[24–26] It is generally accepted that calcium phosphate and glass ceramics are bioactive[27] and make direct contact with bone.[28] On the other hand, titanium and its alloys are biocompatible materials but lack high interfacial bond strengths when compared with bioactive materials.[24] No clear-cut relationship between surface roughness and bond strength exists. However, a general relationship has emerged that indicates that smooth surfaces promote the formation of thick fibrous encapsulation, and rough surfaces favor more intimate bone integration.[29] It is possible that rough surfaces would limit micromotion at the interface; however, a number of other variables[30] may be important. The titanium implant modeled in this study was nonthreaded. Based on a review of the literature,[31,32] it is unlikely that the interface possesses a high shear bond strength. Thus, two extremes were modeled: fully bonded and unbonded. It is likely that in vivo bonding conditions lie between these two extremes.

Only cantilever bending load conditions were simulated. The results indicate that if bonding is assumed, MIN_{pmax} around the implant decreases by approximately 6.5 fold for NA and LA when compared to their respective unbonded models. The lack of a bond could result in relatively high strains, for example, in unbonded LA. Our results concur with those of Siegele and Soltesz[33] and Hipp et al,[34] but contradict the finding of Rieger et al.[35] Siegele and Soltesz[33] demonstrated a 2- to 5-fold increase in the values of maximum compressive stress adjacent to an unbonded implant in comparison with one with a full bond, using a 100 N axial load. Hipp et al[34] emphasize the importance of interfacial bonding assumptions. Their data suggest that an unbonded model would have larger values of maximum stress and greater motion than the bonded model.[36] However, based on results of stress distribution, Rieger et al[35] found no biomechanical advantage to having a fully bonded interface when compared to one that has bone closely adapted to the implant. Clift et al[10] suggest that the results of Reiger et al[35] may be explained by the fact that a nonsophisticated numeric algorithm was used to describe the allowable contact between implant and bone.

Intuitively, we expected MIN_p to be located along the plane of loading (Θ = 0 or 180 degrees) of unbonded NA. However, toward the center of the cortical bone, MIN_p values were located away from the plane of loading. In contrast, MIN_p values for bonded AD were located along or near the plane of loading. This again emphasizes the differences between these two models and the effects of bonding.

Analogies between fracture healing and healing at the implant interface have been made.[5,37] The interfragmentary strain hypothesis attempts to provide a unifying theory to explain the relationship of strain, fracture immobilization, and tissue response.[38] Gardner et al[39] demonstrate that fracture motion triggers callus proliferation. This in turn results in increased stability. Carter et al[40] proposed that the increased constraint may function to decrease strains and to allow bone formation to proceed. Results of the present study demonstrate the importance of calluses in decreasing various mechanical parameters both in unbonded and bonded situations. Calluses decrease MIN_{pmax} by approximately 3 to 7 fold, depending on the interface bonding condition. Brunski[37] suggests that the stability of an implant is paramount in the development of a mineralized versus nonmineralized interface. Thus, reduction in strains by the callus may provide an environment for regeneration.

Endosseous implants are routinely placed with a two-stage procedure in accordance with Brånemark's philosophy.[4] However, histomorphometric data from screw-shaped implants suggest that much earlier[41,42] or even immediate loading may be possible. It has been suggested that improved screw-shaped implant designs with greater retentiveness would decrease micromotion to such a degree that regeneration of bone may be possible even with early loading.[42] However, in this study of a nonthreaded implant, the results clearly demonstrate large differences in strains of the NA and AD model. It would be interesting to develop a similar FE model of a threaded implant. Also, since the maxillary sites for implant placement have thinner cortical bone for supporting implants, the effect of cortical bone thickness on various mechanical parameters should be investigated. Currently, the effects of compressive and torsional loads on the three bonded models are being examined, and comparisons between various mechanical parameters will be made.

Conclusion

Healing response subsequent to implant placement is characterized by formation of calluses, rapid remodeling of bone adjacent to the implant, and an increase in interfacial bond strength. The dramatic effects of these responses on various mechanical parameters are demonstrated in this study. These parameters are considered to be determinants of bone response to mechanical loads. The results suggest the importance of the stabilizing roles provided by the callus and development of a bond during the critical phases of bone healing and long-term adaptation.

Acknowledgments

This work was supported by National Institutes of Dental Research grant PHS R55 DE09822. The assistance by Drs D. B. Burr, J. Chen, L. P. Garetto, and R. Pidaparti is gratefully acknowledged. Assistance by Dentsply (Encino, CA) and Interpore (Irvine, CA) is also appreciated.

References

1. Lazzara R, Siddiqui AA, Binon P, Feldman SA, Weiner R, Phillips R, et al. Retrospective multicenter analysis of 3i endosseous dental implants placed over a five-year period. Clin Oral Implants Res 1996;7:73–83.
2. Jemt T, Lekholm U, Grondahl K. A 3-year follow-up study of early single implant restorations ad modum Brånemark. Int J Periodont Rest Dent 1990;10:341–349.
3. Tjellstrom A. Other applications of osseointegrated implants. In: Brånemark P-I, Zarb GE, Albrektsson T (eds). Tissue-Integrated Prostheses. Chicago: Quintessence, 1985:333–343.
4. Albrektsson T, Lekholm U. Osseointegration: Current state of the art. Dent Clin North Am 1989;33:537–554.
5. Garetto LP, Chen J, Parr JA, Roberts WE. Remodeling dynamics of bone supporting rigidly fixed titanium implants: A histomorphometric comparison in four species including humans. Implant Dent 1995;4:235–243.
6. Hoshaw SJ, Brunski JB, Cochran GVB. Mechanical loading of Brånemark implants affect interfacial bone modeling and remodeling. Int J Oral Maxillofac Implants 1994;9:345–360.
7. Roberts WE. Bone tissue interface. J Dent Educ 1988;52:804–809.
8. Huja SS, Katona TR, Moore BK, Roberts WE. Microhardness and anisotropy of the vital osseous interface and endosseous implant supporting bone. J Orthop Res 1998;16:54–60.
9. Chen J, Lu X, Paydar N, Akay HU, Roberts WE. Mechanical simulation of the human mandible with or without an endosseous implant. Med Eng Phys 1994;16:53–61.
10. Clift SE, Fisher J, Watson CJ. Finite element stress and strain analysis of the bone surrounding a dental implant: Effect of variations in bone modulus. Proc Inst Mech Eng 1992;206:233–241.

11. Huiskes R, Nunamaker DM. Local stresses and bone adaptation around orthopedic implants. Calcif Tissue Int 1984;36:S110–S117.
12. Rubin CT, McLeod KJ. Biological modulation of mechanical influences in bone remodeling. In: Mow VC, Ratcliffe A, Woo SL-Y (eds). Biomechanics of Diarthodial Joints, vol 2. New York: Springer Verlag, 1986:97–118.
13. Roberts WE, Helm FR, Marshall KJ, Gongloff RK. Rigid endosseous implants for orthodontic and orthopedic anchorage. Angle Orthod 1989;59:247–256.
14. ABAQUS/Standard user's manual, vol II. Hibbit, Karlsson & Sorensen, 1995:8.6.1-1–8.6.1-3.
15. Katona TR, Goodacre CJ, Brown DT, Roberts WE. Force-moment systems on single maxillary anterior implants: Effects of incisal guidance, fixture orientation, and loss of bone support. Int J Oral Maxillofac Implants 1993;8:512–522.
16. Ashman RB, Cowin SC, Van Buskirk WC, Rice JC. A continuous wave technique for the measurement of the elastic properties of cortical bone. J Biomech 1984;17:349–361.
17. Keller JC, Lautenschlager EP. Metals and alloys. In: von Recum AF (ed). Handbook of Biomaterials Evaluation—Scientific, Technical, and Clinical Testing of Implant Materials. New York: Macmillan, 1986:19.
18. Rho JY, Ashman RB, Turner CH. Young's modulus of trabecular and cortical bone material: Ultrasonic and microtensile measurements. J Biomech 1993;26:111–119.
19. Takano Y, Turner CH, Burr DB. Mineral anisotropy in mineralized tissues is similar among species and mineral growth occurs independently of collagen orientation in rats: Results from acoustic velocity measurements. J Bone Miner Res 1996;11:1292–1301.
20. Harten RD Jr, Depaula CA, Kotha S, Zimmerman MC, Parsons JR, Guzelsu N. The relationship between cortical bone elasticity and acoustic impedance. Minneapolis: Society for Biomaterials, 1997.
21. Harten RD Jr, Lee FY, Zimmerman MC, Hurowitz E, Arakal R, Behrens FF. Regional and temporal changes in the acoustic properties of fracture callus in secondary bone healing. J Orthop Res 1997;15:570–576.
22. Currey JD, Brear K. Hardness, Young's modulus and yield stress in mammalian mineralized tissue. J Mater Sci Mater Med 1990;1:14–20.
23. Evans GP, Behiri JC, Bonfield W. Microhardness, Young's modulus and mineral content in bone and bone analogue. In: de Putter C, de Lange GL, de Groot K, Lee AJC (eds). Implant Materials in Biofunction: Advances in Biomaterials, vol 8. Amsterdam: Elsevier Science Publishers BV, 1988:311–315.
24. Cook SD, Kay JF, Thomas KA, Jarcho M. Interface mechanics and histology of titanium and hydroxylapatite-coated titanium for dental implant applications. Int J Oral Maxillofac Implants 1987;2:15–22.
25. Takatsuka K, Yamamuro T, Nakamura T, Kukubo T. Bone-bonding behavior of titanium alloy evaluated mechanically with detaching failure load. J Biomed Mater Res 1995;29:157–163.
26. De Groot K. Letters to the Editor. J Biomed Mater Res 1989;23:1367–1371.
27. Niki M, Ito G, Matsuda T, Ogino M. Comparative push-out data of bioactive and non-bioactive materials of similar rugosity. In: Davies JE (ed). The Bone-Biomaterial Interface. Toronto: Univ of Toronto Press, 1991:350–356.
28. Hench LL, Splinter RJ, Greenle TK, Allen WC. Bonding mechanisms at the interface of ceramic prosthetic materials. J Biomed Mater Res Symp 1971;2:117–141.
29. Ricci JL, Spivak JM, Blumenthal NC, Alexander H. Modulation of bone ingrowth by surface chemistry and roughness. In: Davies JE (ed). The Bone-Biomaterial Interface. Toronto: Univ of Toronto Press, 1991:334–349.
30. Brunski JB, Moccia AF Jr, Pollack SR, Korostoff E, Trachtenberg DI. The influence of functional use of endosseous dental implants on the tissue-implant interface. I. Clinical aspects. J Dent Res 1979;50:1970–1980.
31. Kitsugi T, Nakamura T, Oka M, Yan W-Q, Goto T, Shibuya T, et al. Bone bonding behavior of titanium and its alloys when coated with titanium oxide (TiO_2) and titanium silicate (Ti_5Si_3). J Biomed Mater Res 1996;32:149–156.
32. Cook SD, Thomas KA, Kay JF, Jarcho M. Hydroxyapatite-coated titanium for orthopedic implant applications. Clin Orthop Rel Res 1988;232:225–243.
33. Siegele D, Soltesz U. Numerical investigations of the influence of implant shape on stress distribution in the jaw bone. Int J Oral Maxillofac Implants 1989;4:333–340.
34. Hipp JA, Brunski JB, Shephard MS, Cochran GVB. Finite element models of implants in bone: Interfacial assumptions. In: Perren SM, Schneider E (eds). Biomechanics: Current Interdisciplinary Research. Dordrecht: Marinus Nijhoff Publishers, 1984:447–452.
35. Rieger MR, Adams WK, Kinzel GL, Brose MO. Finite element analysis of bone-adapted and bone-bonded endosseous implants. J Prosthet Dent 1989;62:436–440.
36. Brunski JB, Moccia AF Jr, Pollack SR, Korostoff E, Trachtenberg DI. The influence of functional use of endosseous dental implants on the tissue-implant interface. I. Histological aspects. J Dent Res 1979;50:1953–1969.
37. Brunski JB. Influence of biomechanical factors at the bone-biomaterial interface. In: Davies JE (ed). The Bone-Biomaterial Interface. Toronto: Univ of Toronto Press, 1991:391–404.
38. Perren SM. Physical and biological aspects of fracture healing with special reference to internal fixation. Clin Orthop Rel Res 1979;138:175–196.
39. Gardner TN, Hardy J, Evans M, Kenwright J. Temporal changes in dynamic interfragmentary motion and callus formation in fractures. J Biomech 1997;30:315–321.
40. Carter DR, Blenman PR, Beaupre GS. Correlations between mechanical stress history and tissue differentiation in initial fracture healing. J Orthop Res 1988;6:736–748.
41. Piattelli A, Corigliano M, Scarano A. Microscopical observations of the osseous responses in early loading human titanium implants: A report of two cases. Biomaterials 1996;17:1333–1337.
42. Piattelli A, Ruggeri A, Franchi M, Romansco N, Trisi P. An histologic and histomorphometric study of bone reactions to unloaded and loaded non-submerged single implants in monkey: A pilot study. J Oral Implantol 1993;14:314–320.